Electronic Supplementary Information

A facile and scale-up synthetic method for covalent organic nanosheets: ultrasonic polycondensation and photocatalytic degradation of organic pollutants

Shi-Xian Gan, Chao Jia, Qiao-Yan Qi, and Xin Zhao

Key Laboratory of Synthetic and Self-Assembly Chemistry for Organic Functional Molecules, Center for Excellence in Molecular Synthesis, Shanghai Institute of Organic Chemistry, University of Chinese Academy of Sciences, Chinese Academy of Sciences, 345 Lingling Road, Shanghai 200032, China

Experimental Details

Materials and Methods

All the reagents and solvents were purchased from commercial suppliers and used without further purification unless otherwise noted. The CONs were synthesized using an ultrasonic cleaner (Shumei KQ-100DB) with a powder output 100 W and a frequency of 40 KHz. Fourier transform infrared spectroscopy (FT-IR) was carried out with a Nicolet 380 FT-IR spectrometer. The samples for the IR study were prepared as KBr pellets. Transmission electron microscopy (TEM) was performed on a JEOL JEM-2100 instrument. Atomic force microscope (AFM) (Bruker, Germany) analysis of the 2D CONs were acquired with tapping mode, for which the samples were prepared by depositing a droplet of dispersion on a freshly cleaved mica surface and dried at room temperature in a vacuum drying oven. Powder X-ray diffraction measurements were carried out with an X' Pert PROX system using monochromated Cu/Kα (λ = 0.1542 nm). The samples were spread on the square recess of a XRD

sample holder as a thin layer. Nitrogen adsorption-desorption measurements were carried out using a *Quantachrome autosord IQ* automatic volumetric instrument. Before gas adsorption measurements, the as-prepared samples (~40 mg) were washed with anhydrous acetone through Soxhlet extraction for 6 h. The solvent was filtered and the samples were activated under vacuum at 120 ℃ for 8 h. Then the samples were used for gas adsorption-desorption measurements from 0 to 1 atm at 77 K. The Brunauer-Emmett-Teller (BET) method was utilizes to calculate their specific surface areas. By using the quenched solid state density functional theory, the pore distributions were derived from the sorption data. A 300 W xenon arc lamp with power density of 2.2 W/cm^2 (at a distance of 25 cm) where a cut-off filter 400 nm has been used to remove UV light was used as the light source for the catalytic dye degradation experiments. UV-Vis spectra for the dyes were collected on a WFZ UV-4802 spectrometer. Solid-sate UV/Vis spectra were recorded using a UH4150 spectrophotometer. The optical band gaps were determined by Tauc's plot method.

Synthesis and characterization

Synthesis of **P-COF** and **T-COF**

The two COFs were synthesized according to a procedure reported in literature with a few modifications.[1] 1,3,5-tris(4-aminophenyl)-benzene(**TAPB**) (35.0 mg, 0.10 mmol), 1,3,5-benzenetricarbaldehyde (**BTCA**) (16.2 mg, 0.10 mmol), and 1,4-dioxane (2.0 mL) were added in a glass ampoule. Then the glass ampoule was immersed in an ultrasonic bath and sonicated for 20 min. After that, aqueous acetic (6.0 M, 0.20 mL) was added and the ampoule was sealed after being degassed in a liquid nitrogen bath for 20 min. The ampoule was warmed to room temperature and then kept at 120 ℃ without disturbance for 7 days to yield a yellow solid at the bottom of the ampoule. After cooled to room temperature, the precipitate was filtered, and the solid was washed with anhydrous dichloromethane, anhydrous acetone and tetrahydrofuran in turn for 3 times, and then activated at 120 ℃ under vacuum for 8 h to afford **P-COF** as yellow powder (43.5 mg, 94.6%).

T-COF (43.7 mg, 93.9%) was synthesized in mesitylene/1,4-dioxane (v/v = 1/9, 2.0 mL) through the condensation of 2,4,6-tris(4-aminophenyl)-1,3,5-triazine (**TAPT**) (35.0 mg, 0.10 mmol) and 1,3,5-benzenetricarbaldehyde (**BTCA**) (16.2 mg, 0.10 mmol), with the same synthetic procedure as that of **P-COF**.

Synthesis of **P-CON**, **T-CON, Tp-P-CON and Tp-T-CON**

To a mixture of 1,3,5-tris(4-aminophenyl)-benzene(**TAPB**) (1.05 g, 2.98 mmol) and 1,3,5-benzenetricarbaldehyde (**BTCA**) (484.4 mg, 2.98 mmol) in a beaker, a mixture of 1,4-dioxane (100 mL) and aqueous acetic (10 mL, 6.0 M) was added. The mixture was immersed in an ultrasonic bath and sonicated in an ice water bath for 8 h (100W, 40 KHz) to yield a very fluffy yellow solid, which swells in the entire solvent system. The solid was filtered, washed with anhydrous dichloromethane, anhydrous acetone and tetrahydrofuran in turn for 3 times, and activated at 120 ℃ under vacuum for 8 h to give ultrathin **P-CON** (1.28 g, 93.4%).

T-CON (1.26 g, 90.6%) was synthesized in mesitylene/1,4-dioxane (v/v = 1/9, 100 mL) through the condensation of 2,4,6-tris(4-aminophenyl)-1,3,5-triazine (**TAPT**) (1.05 g, 2.98 mmol) and 1,3,5-benzenetricarbaldehyde (**BTCA**) (484.4 mg, 2.98 mmol), with the same synthetic procedure as that of **P-CON**.

Tp-P-CON (69.8 mg, 80.9%) was synthesized in 1,4-dioxane (2.0 mL) through the condensation of 1,3,5-tris(4-aminophenyl)-benzene(**TAPB**) (58.5 mg, 0.17 mmol) and 1,3,5-triformylphloroglucinol (**Tp**) (35.0 mg, 0.17 mmol), with the same synthetic procedure as that of **P-CON**.

Tp-T-CON (72.9 mg, 84.1%) was synthesized in 1,4-dioxane (2.0 mL) through the condensation of 2,4,6-tris(4-aminophenyl)-1,3,5-triazine (**TAPT**) (59.0 mg, 0.17mmol) and 1,3,5-triformylphloroglucinol (**Tp**) (35.0 mg, 0.17 mmol), with the same synthetic procedure as that of **P-CON**.

Photocatalytic Investigations

The photocatalytic degradation of methylene blue (**MB**) and thionine acetate salt (**Th**) in water (10 mg/L) was performed under a xenon arc lamp (300W) irradiation at ambient temperature and pressure. In a 100 mL sandwich beaker, **T-CON** or **P-CON** (25 mg) was dispersed in the corresponding dye aqueous solution (50 mL). Circulated water was used to maintain the entire reaction process at room temperature. The dye solution along with the catalyst was stirred under dark for 90 min for the achievement of adsorption-desorption equilibrium prior to introduction of visible light source. The entire reaction was performed under visible light irradiation during the course of the photocatalytic experiment. An aliquot of the reaction mixture (0.70 mL) was taken by a pipette every 30 min to monitor the degradation process, for which the catalyst was removed through centrifuge and the supernatant was examined to give the concentration of the dye with an ultraviolet-visible spectrophotometer. The degradation efficiency (%) was calculated from equation listed below:

$$\text{Degradation efficiency (\%)} = \frac{C_0 - C_t}{C_0} \times 100$$

Where C_0 and C_t are the concentrations of dye at t = 0 and t minutes of photocatalytic reaction, respectively.

After each run of the photocatalytic experiments, the solutions were filtered to recover the CON catalysts, and a large amount of water and ethanol were used to wash the catalysts to ensure that the adsorbed dyes were removed. Then, the recovered catalysts were active under vacuum at 80 ℃ for 4 h, and examined by PXRD before being used in the next run. To ensure the accuracy of the experiments, each cycle experiment was performed under the same condition.

Reference

1. J. Q. Dong, Y. X. Wang, G. L. Liu, Y. D. Cheng and D. Zhao, *CrystEngcomm.*, 2017, **19**, 4899-4904.

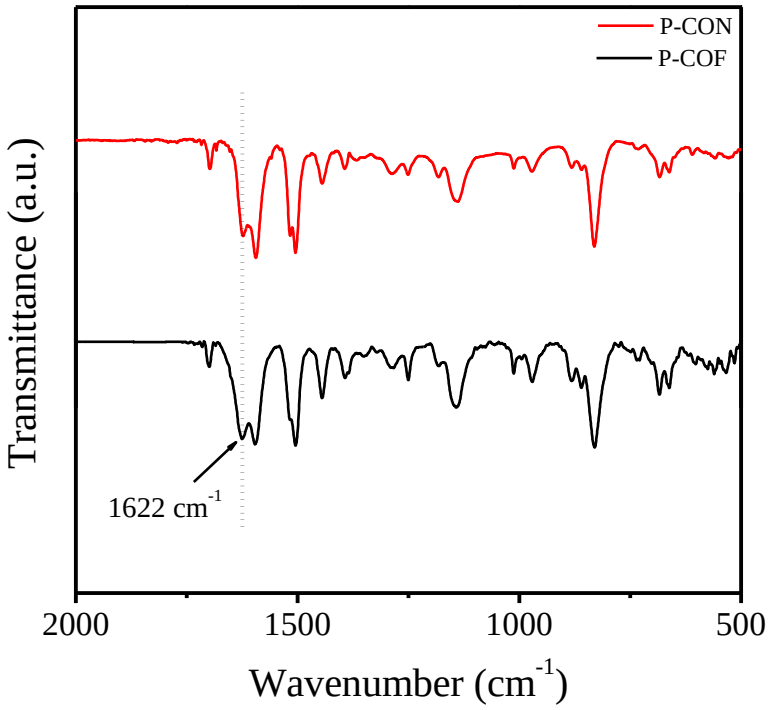

Fig. S1 FT-IR spectra of **P-COF** (black) and **P-CON** (red).

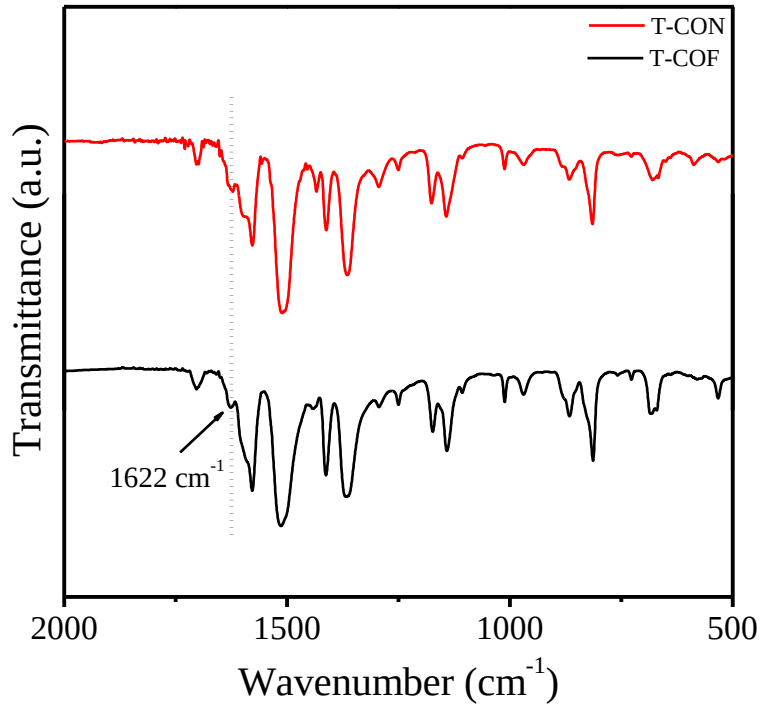

Fig. S2 FT-IR spectra of **T-COF** (black) and **T-CON** (red).

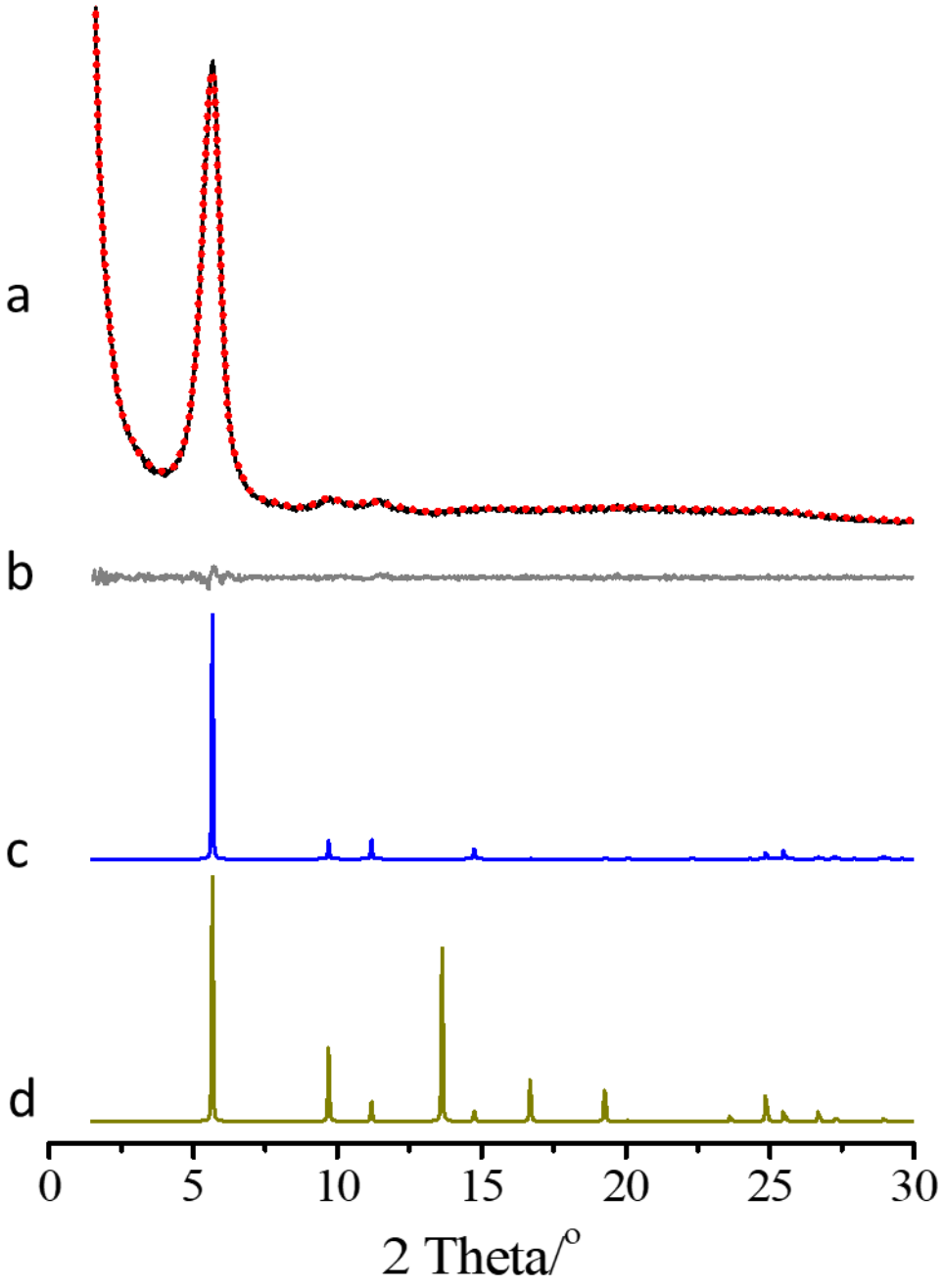

Fig. S3 (a) Experimental (black) and refined (red) PXRD patterns of **P-COF**. (b) Difference plot between the experimental and refined PXRD patterns. Simulated PXRD patterns for the predicted COF structure with eclipsed (c) and staggered stacking models (d).

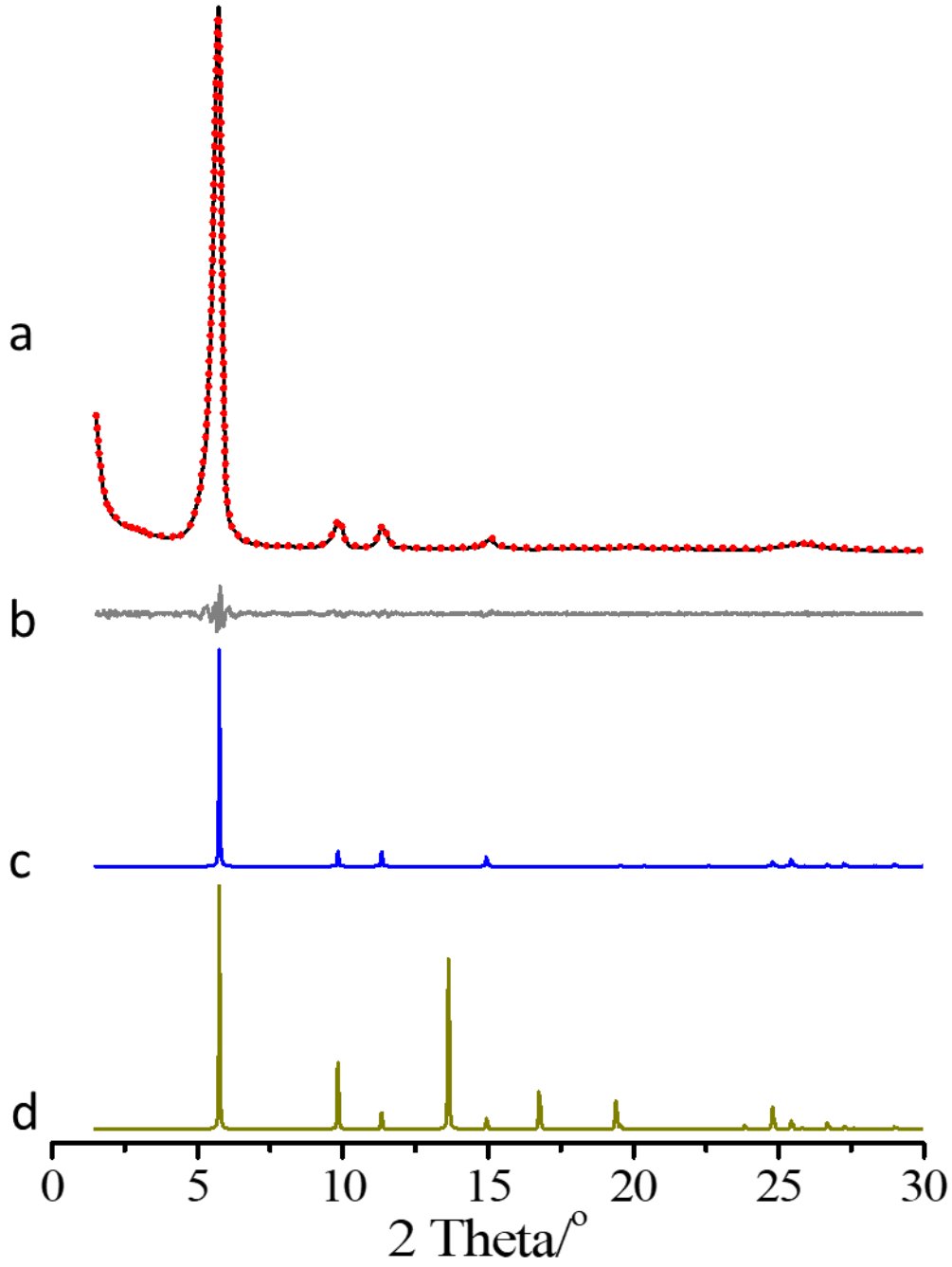

Fig. S4 (a) Experimental (black) and refined (red) PXRD patterns of **T-COF**. (b) Difference plot between the experimental and refined PXRD patterns. Simulated PXRD patterns for the predicted COF structure with eclipsed (c) and staggered stacking models (d).

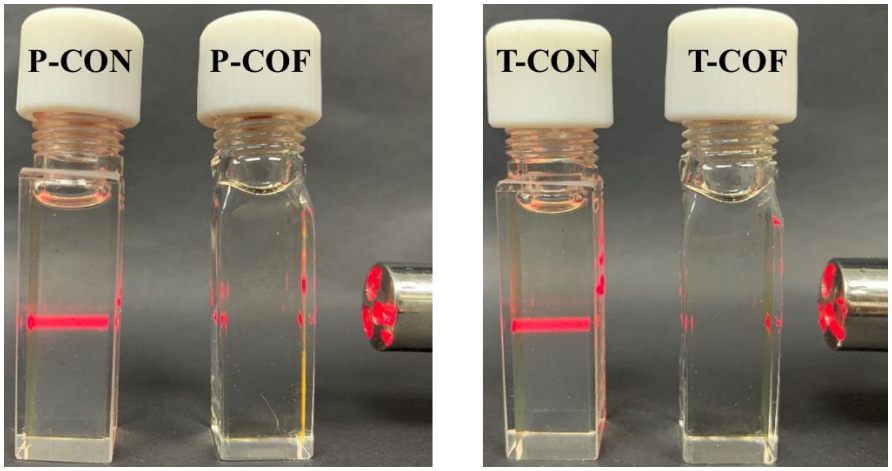

Fig. S5 Photographs recorded for testing Tundall effect of CONs and COFs after the samples were stood for two months.

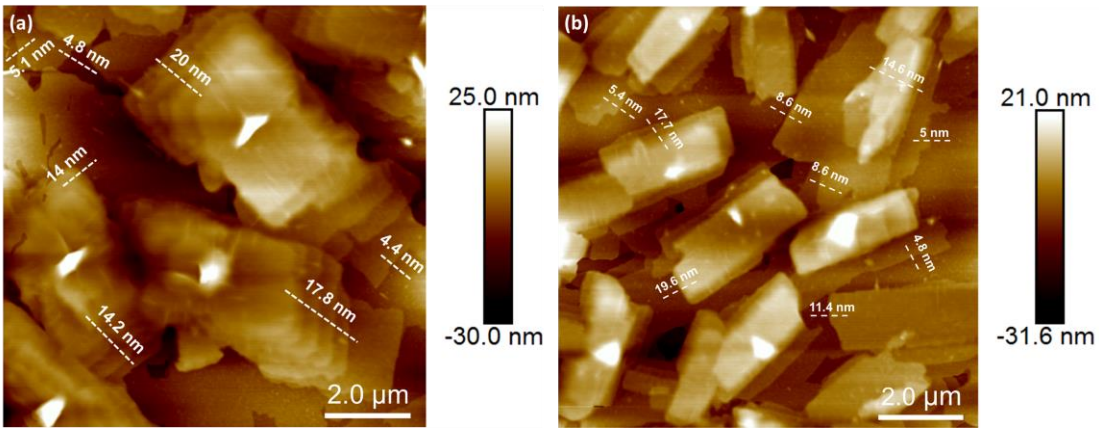

Fig. S6 2D model of AFM images of **P-CON** (a) and **T-CON** (b).

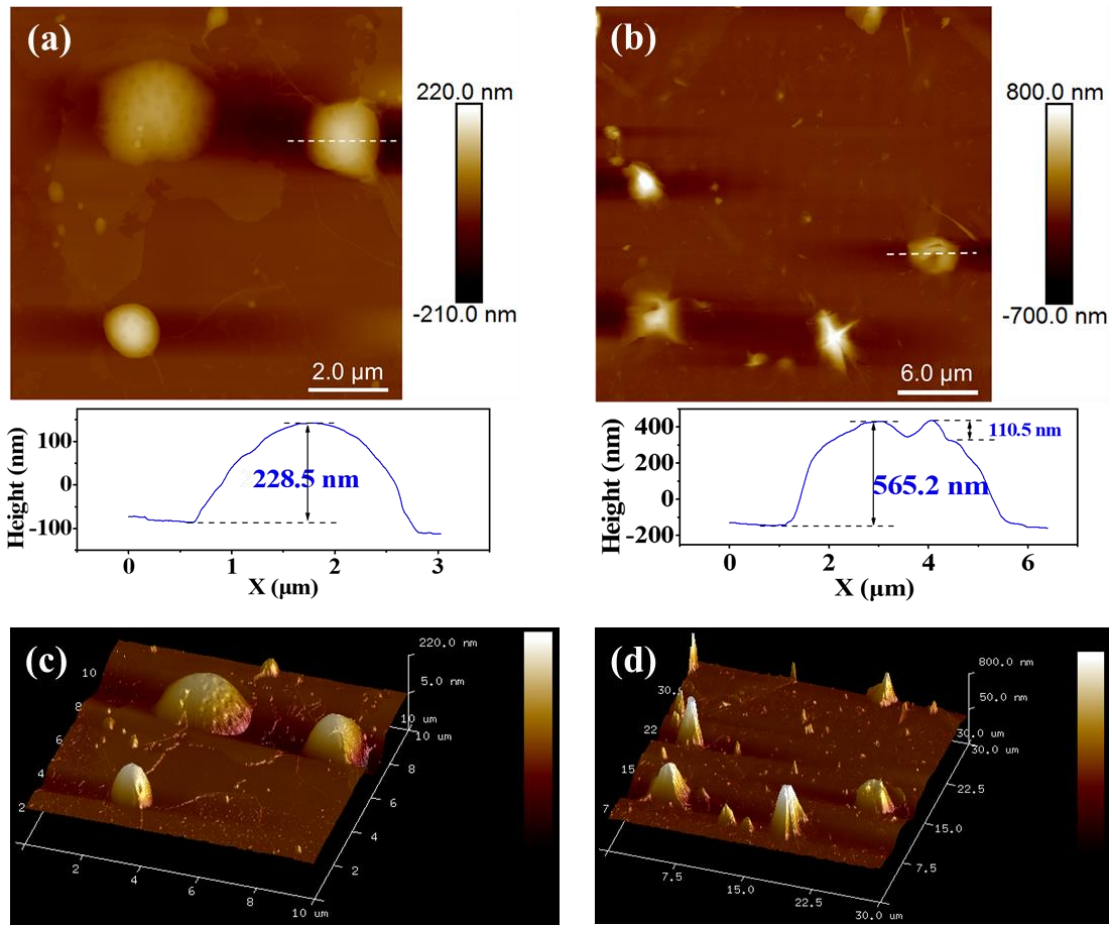

Fig. S7 2D model of AFM images of **P-COF** (a) and **T-COF** (b), and 3D model of AFM images of **P-COF** (c) and **T-COF** (d).

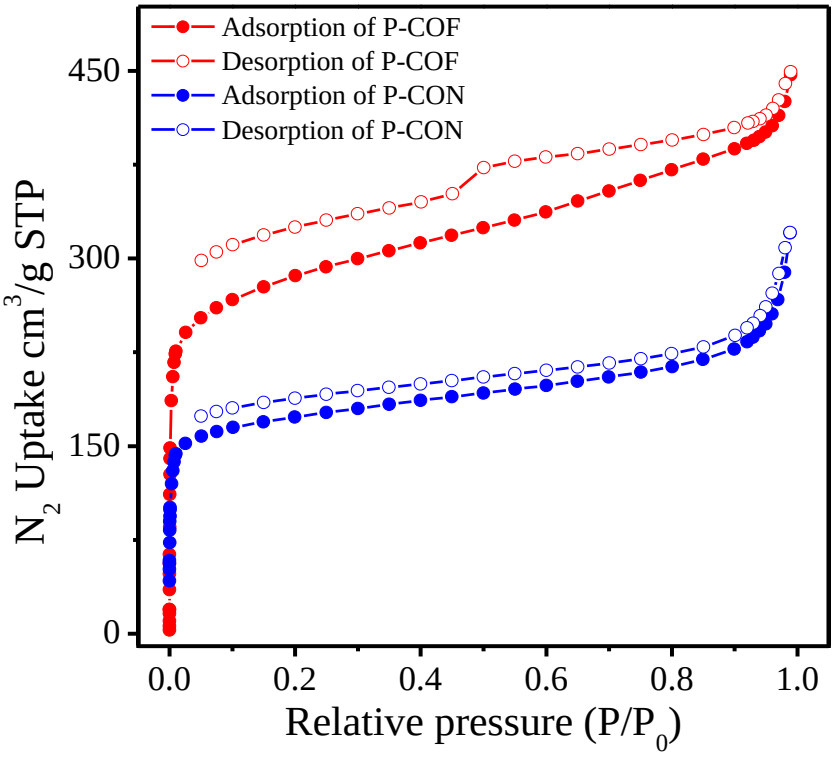

Fig. S8 N_2 adsorption-desorption isotherms of **P-COF** (red) and **P-CON** (blue).

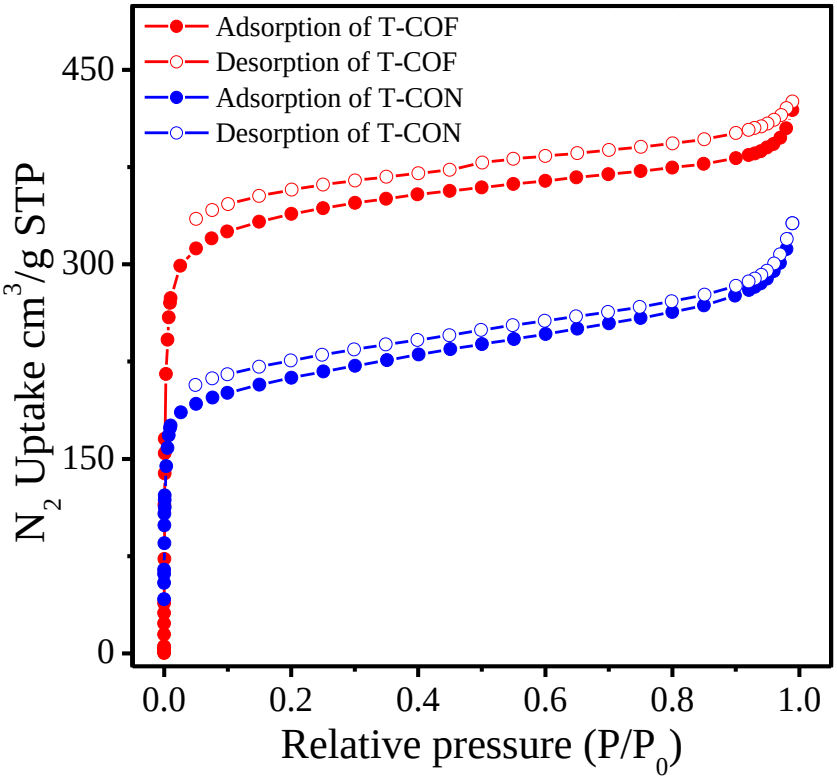

Fig. S9 N_2 adsorption-desorption isotherms of **T-COF** (red) and **T-CON** (blue).

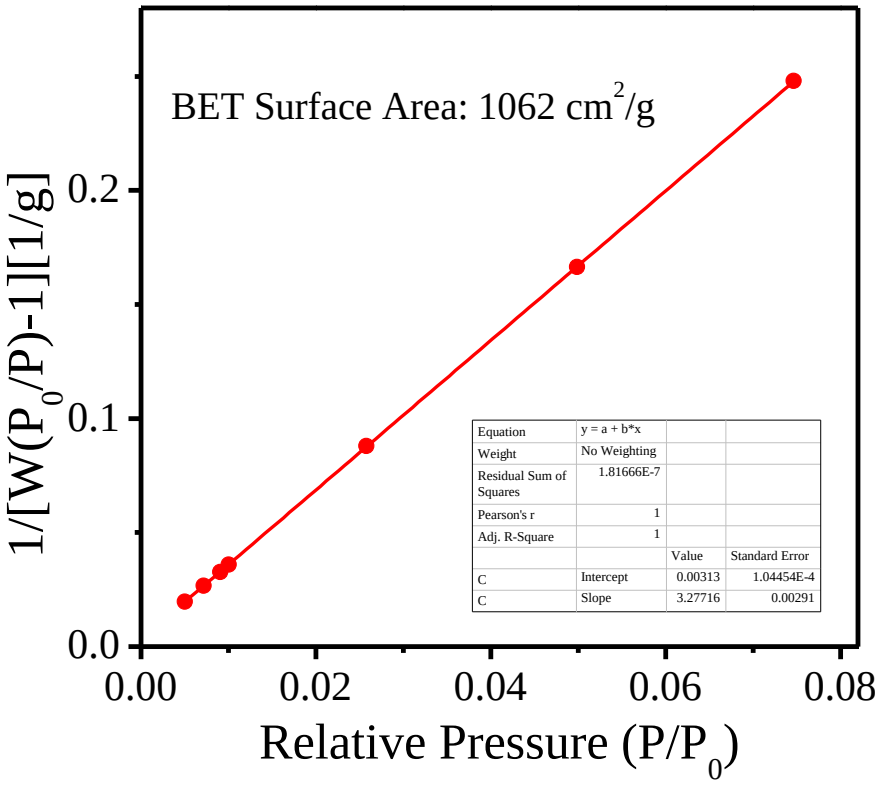

Fig. S10 BET surface area plot for **P-COF** calculated from the adsorption data.

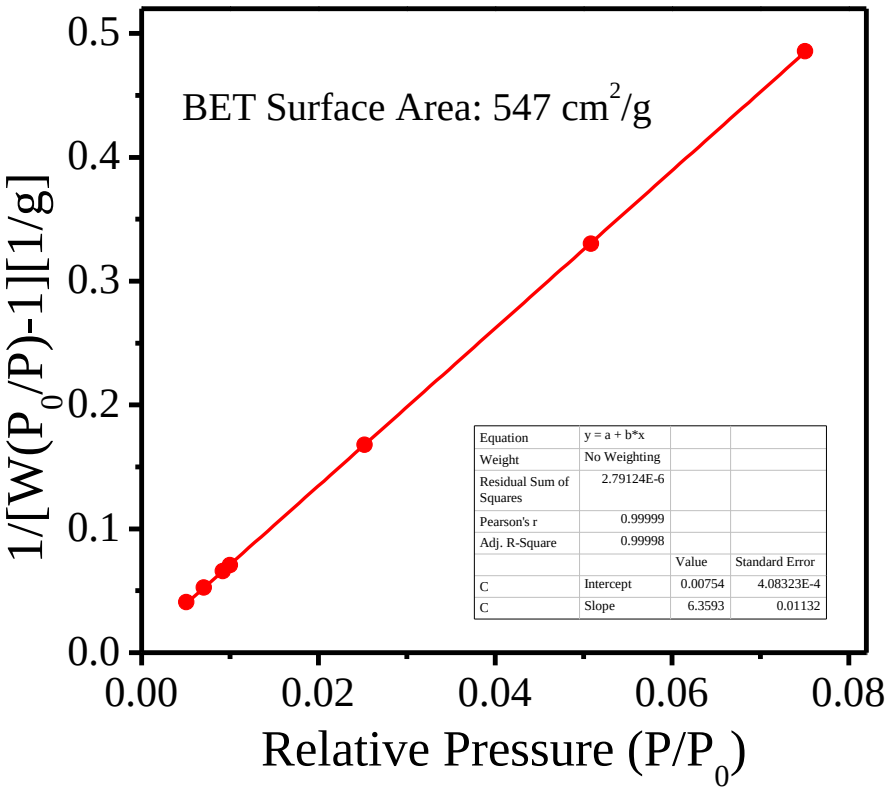

Fig. S11 BET surface area plot for **P-CON** calculated from the adsorption data.

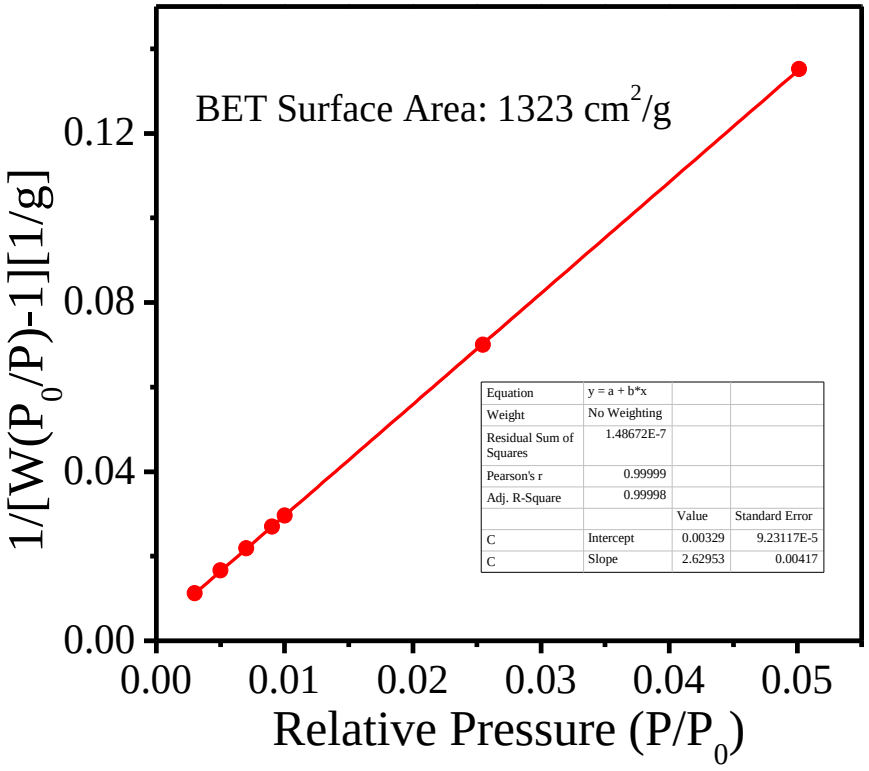

Fig. S12 BET surface area plot for **T-COF** calculated from the adsorption data.

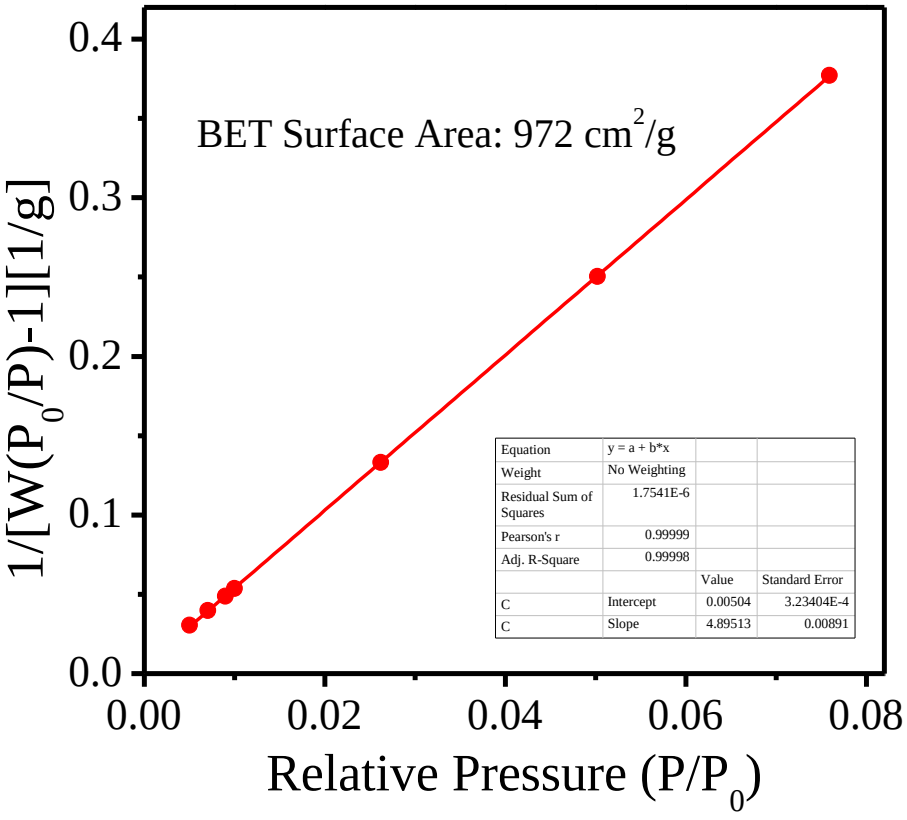

Fig. S13 BET surface area plot for **T-CON** calculated from the adsorption data.

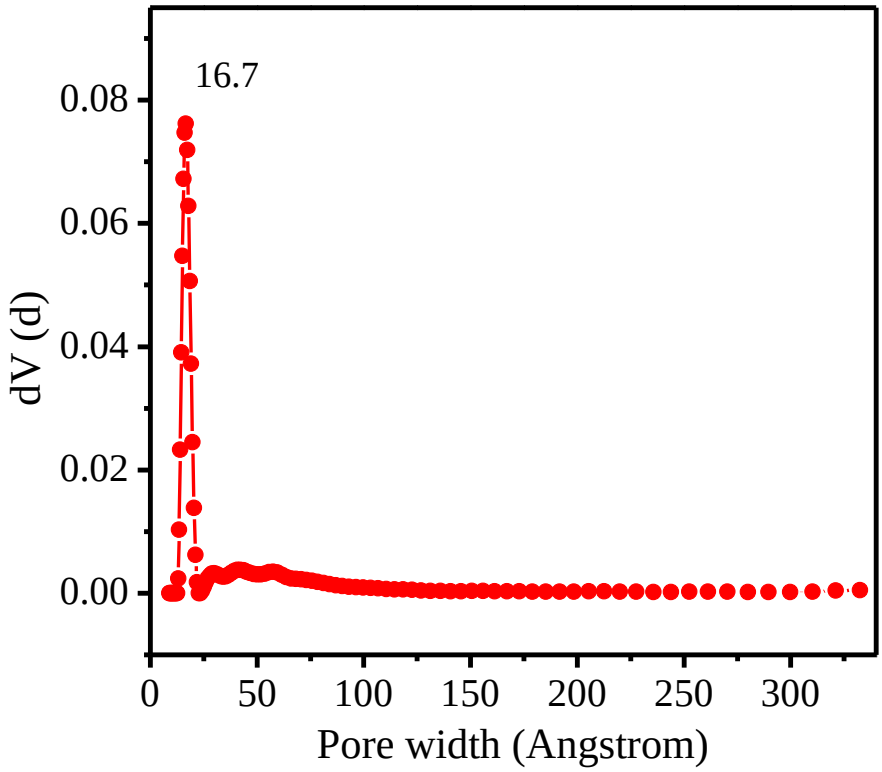

Fig. S14 Pore size distribution profile of **P-COF**.

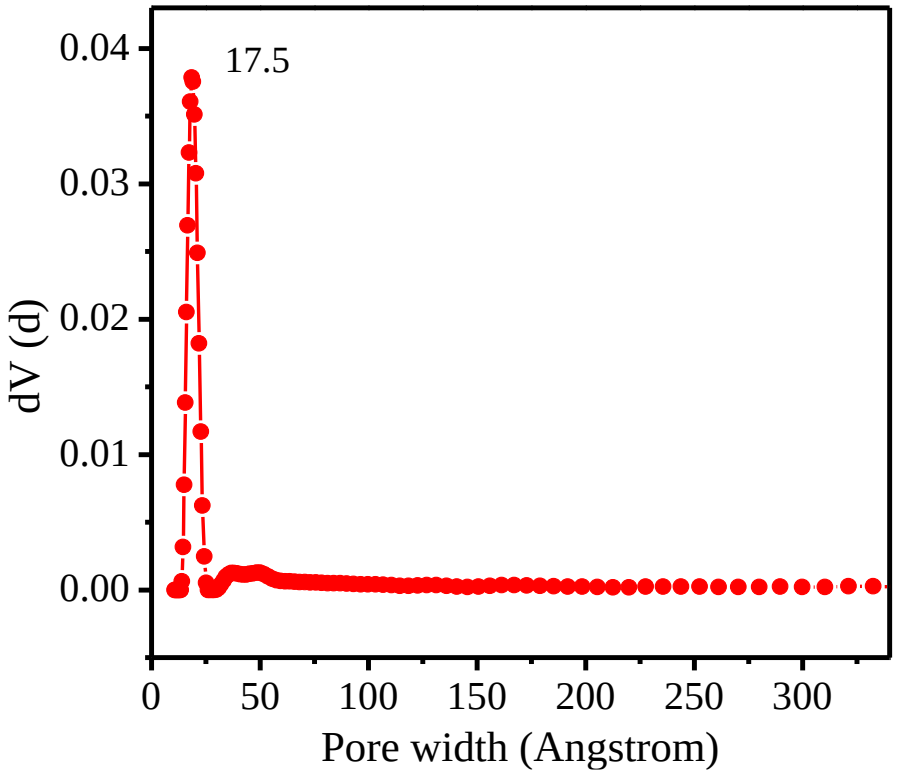

Fig. S15 Pore size distribution profile of **P-CON**.

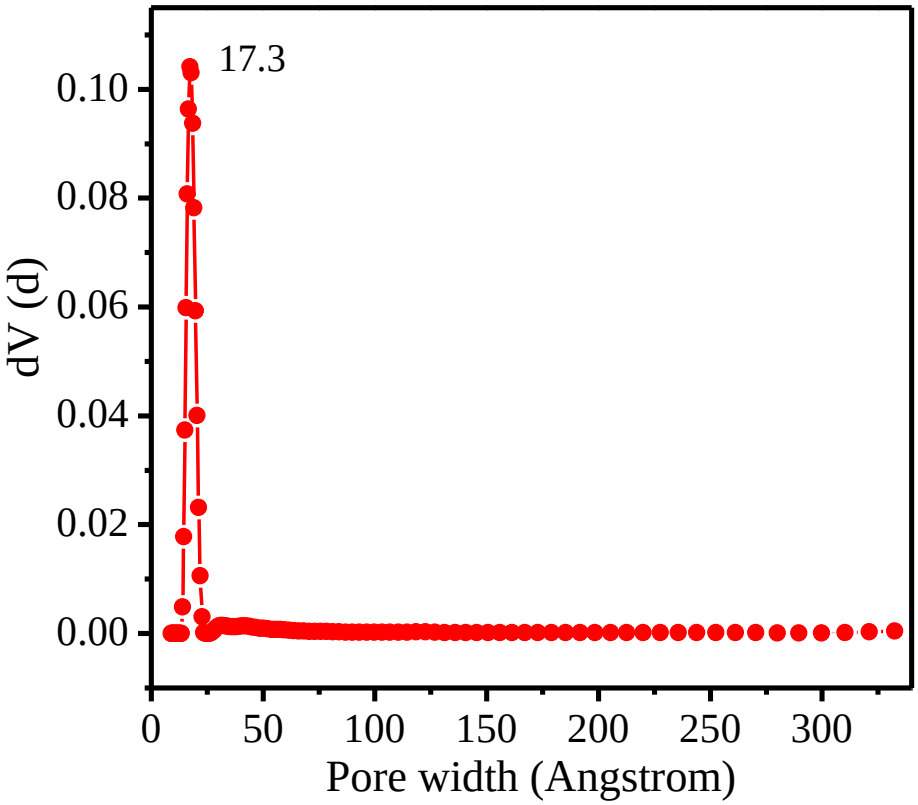

Fig. S16 Pore size distribution profile of **T-COF**.

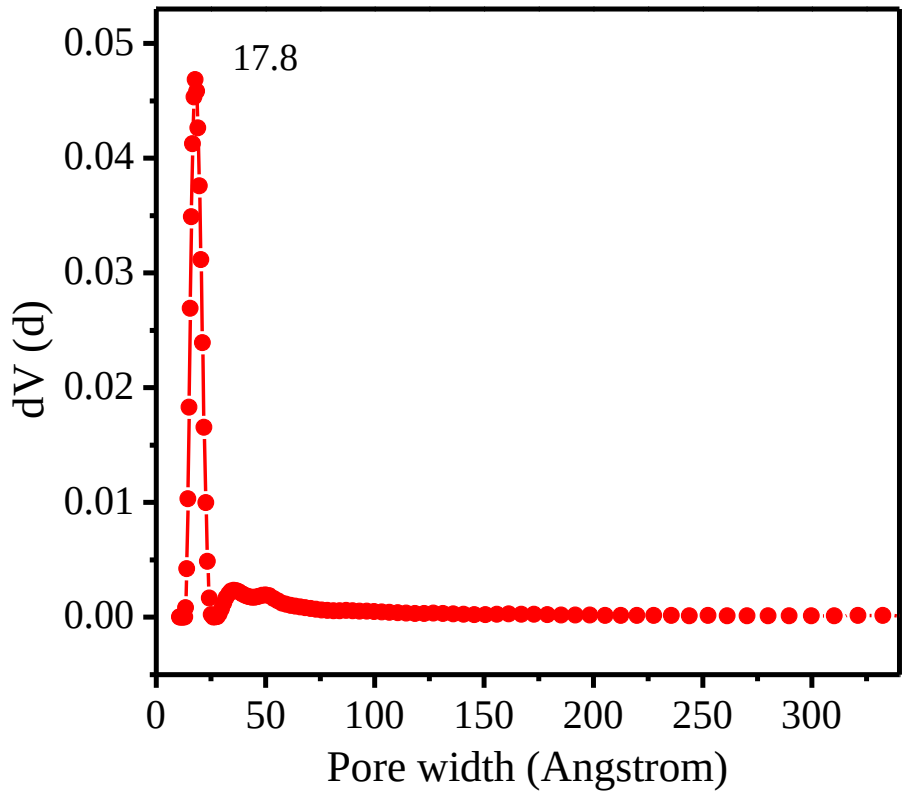

Fig. S17 Pore size distribution profile of **T-CON**.

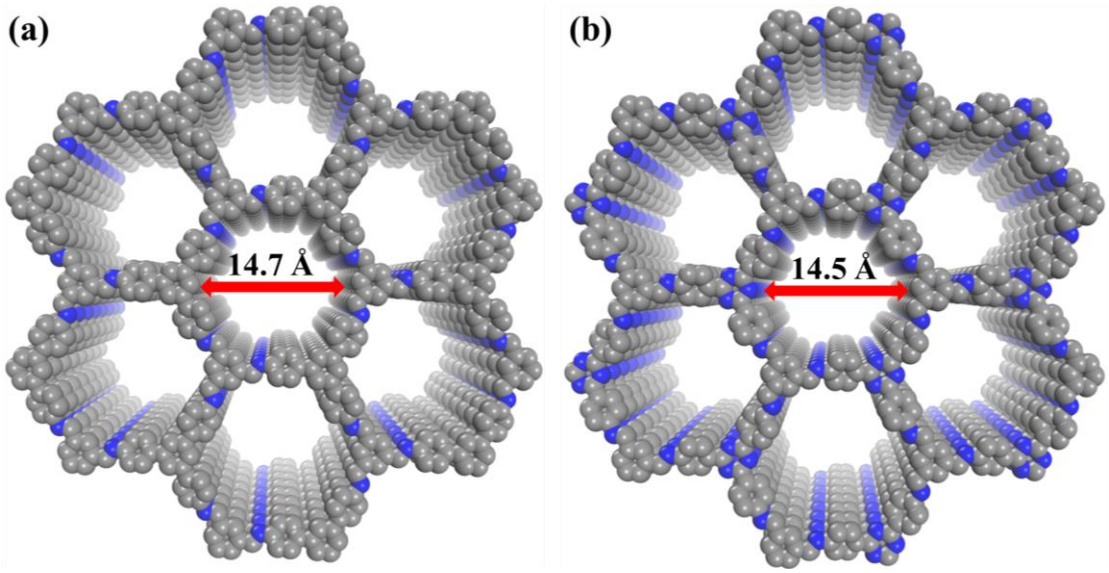

Fig. S18 Illustration for theoretical pore sizes of **P-COF** (a) and **T-COF** (b).

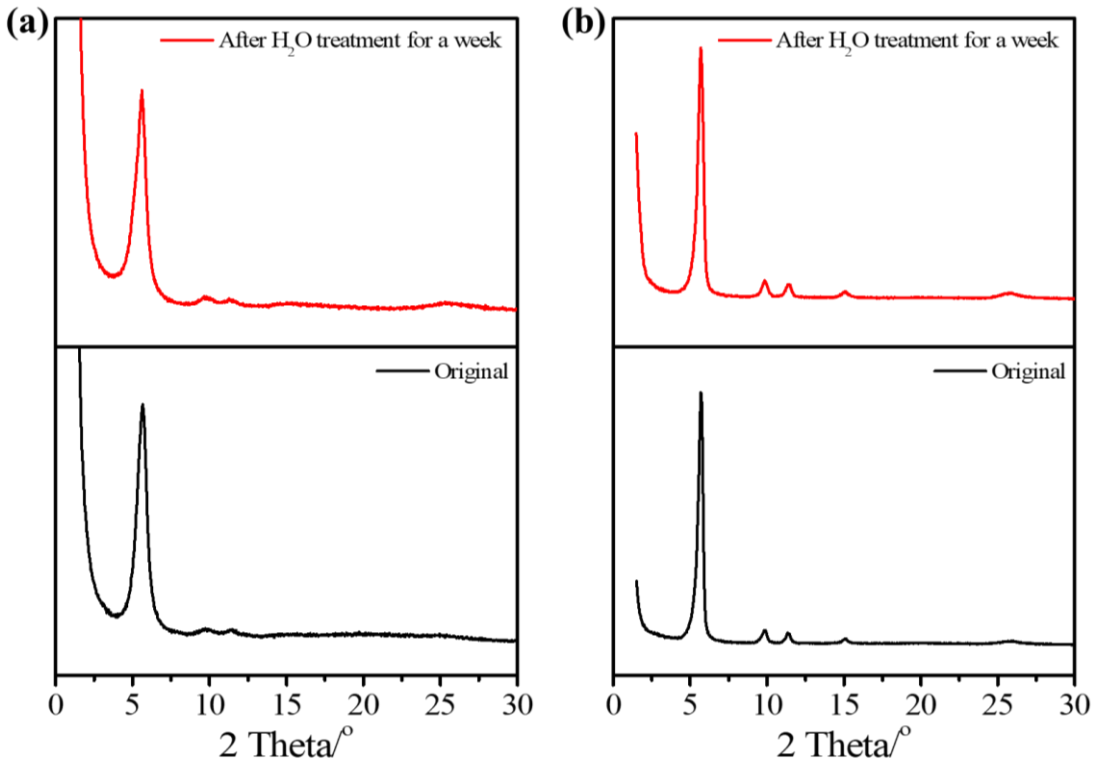

Fig. S19 PXRD patterns of **P-COF** (a) and **T-COF** (b) after they were immersed in H_2O for a week. The original PXRD profiles are also provided for comparison.

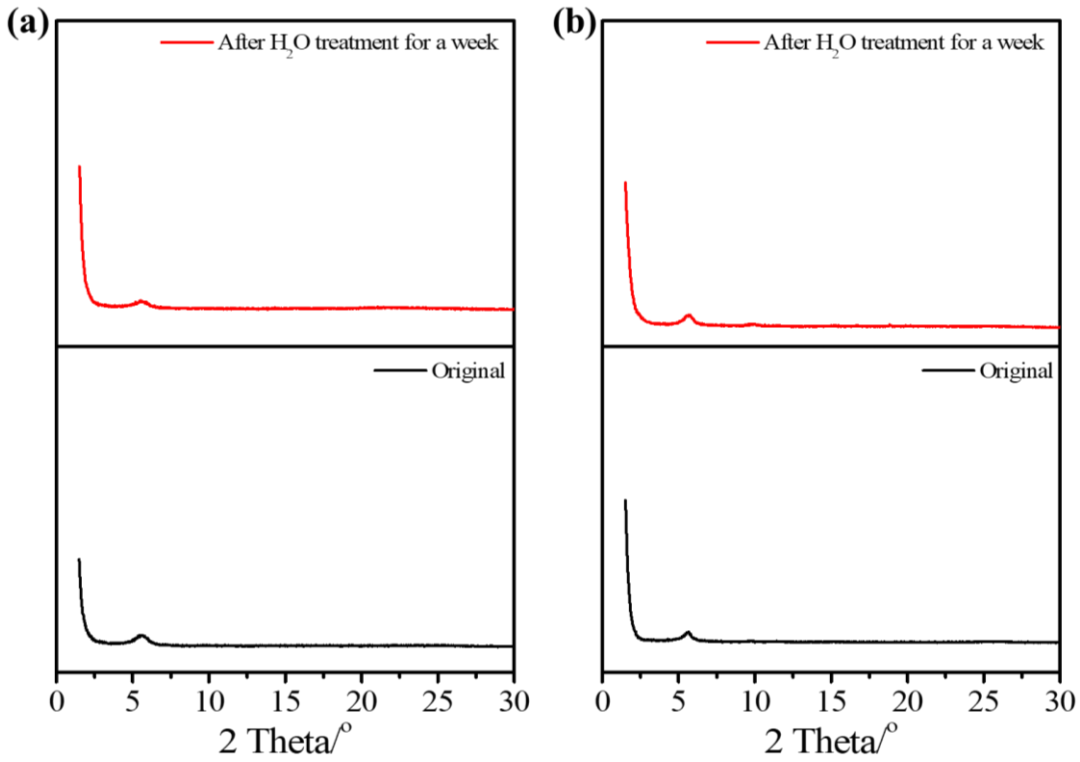

Fig. S20 PXRD patterns of **P-CON** (a) and **T-CON** (b) after they were immersed in H_2O for a week. The original PXRD profiles are also provided for comparison.

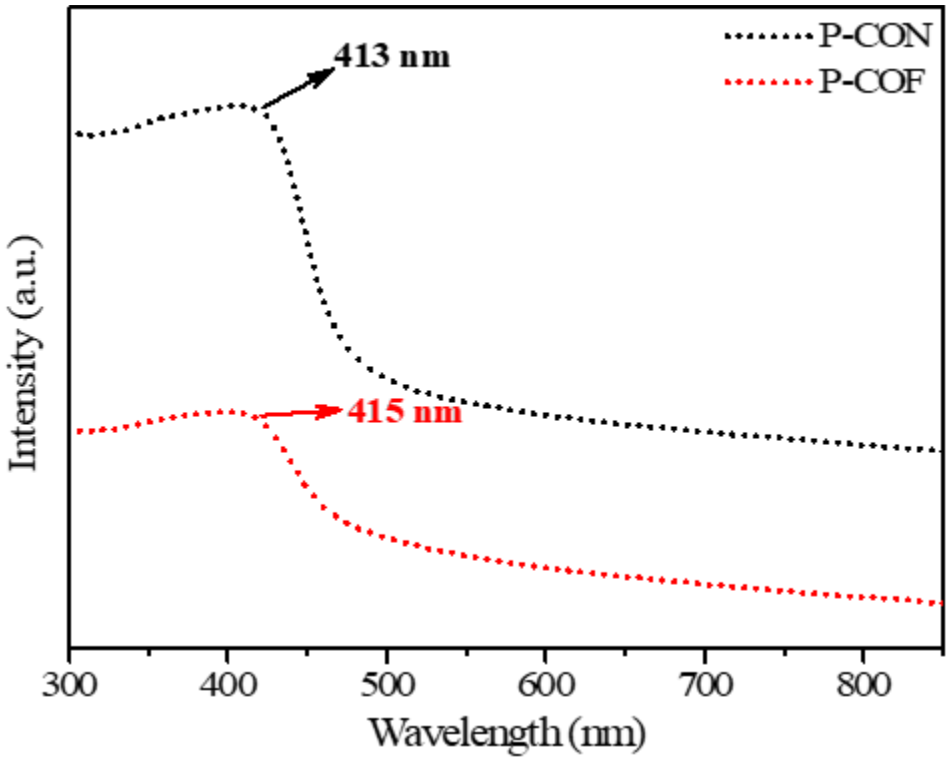

Fig. S21 UV-Vis DRS spectra of **P-CON** (black) and **P-COF** (red).

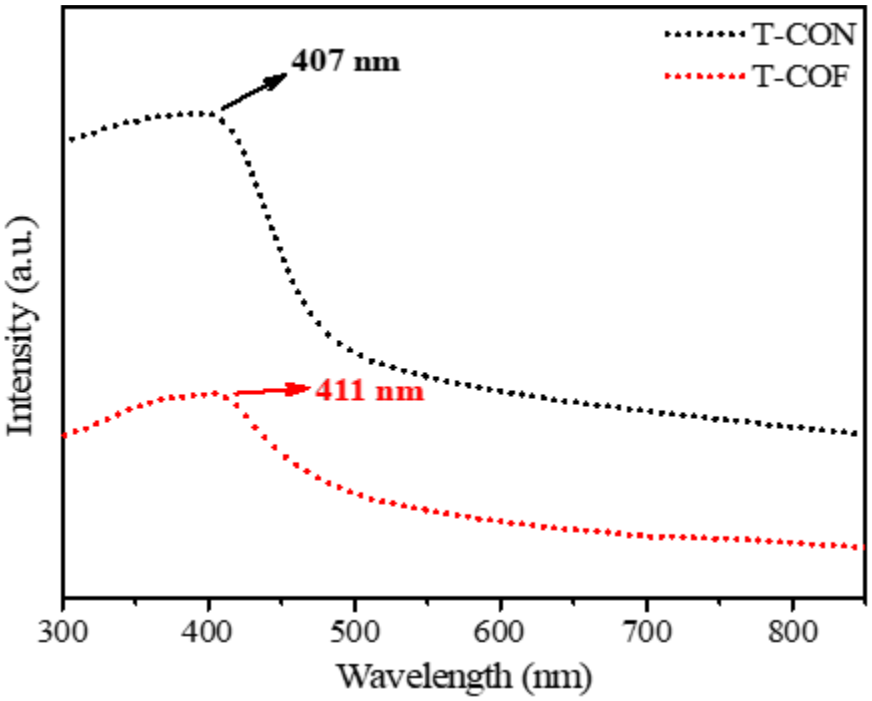

Fig. S22 UV-Vis DRS spectra of **T-CON** (black) and **T-COF** (red).

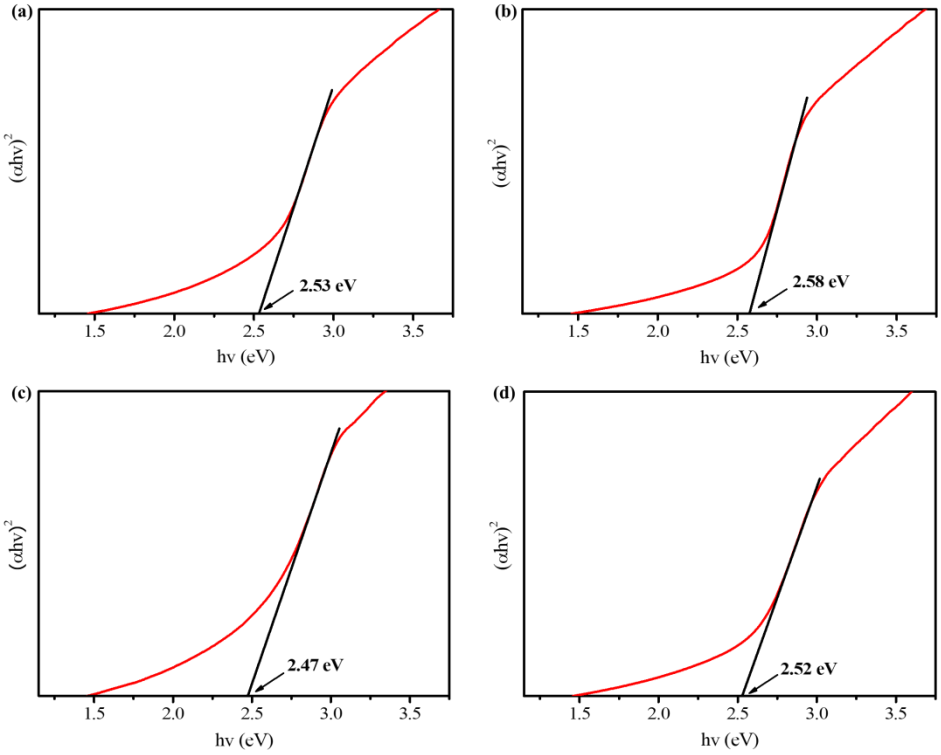

Fig. S23 Energy band gaps of **P-COF** (a), **P-CON** (b), **T-COF** (c) and **T-CON** (d) derived from Tauc's relation.

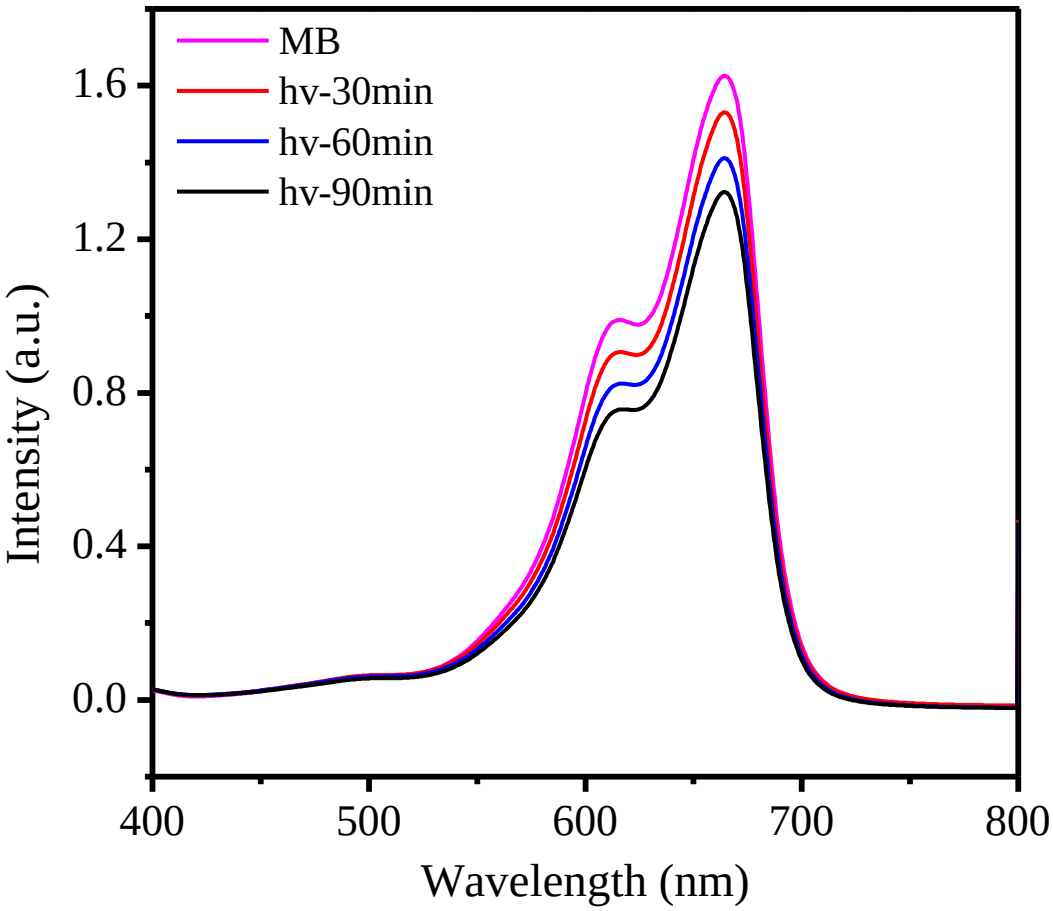

Fig. S24 UV-Vis spectra of a **MB** aqueous solution under visible light irradiation for different time.

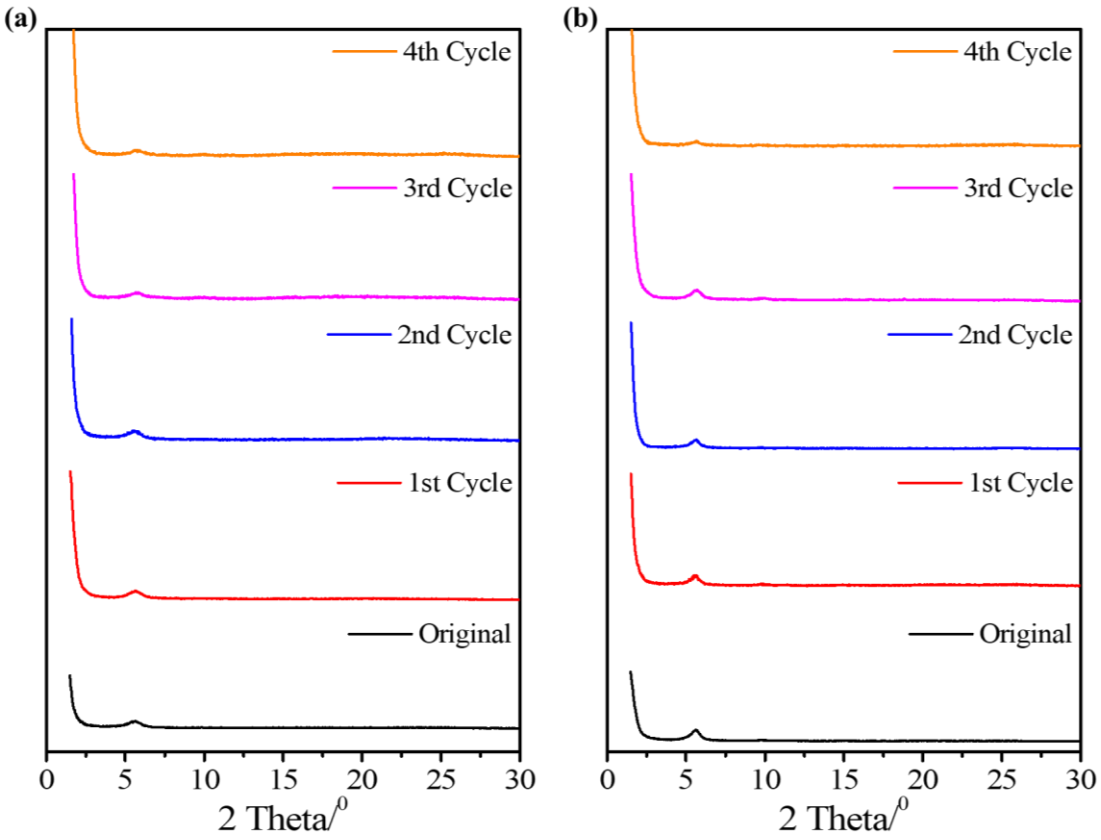

Fig. S25 PXRD patterns of **P-CON** (a) and **T-CON** (b) after each cycle of the **MB** degradation experiment.

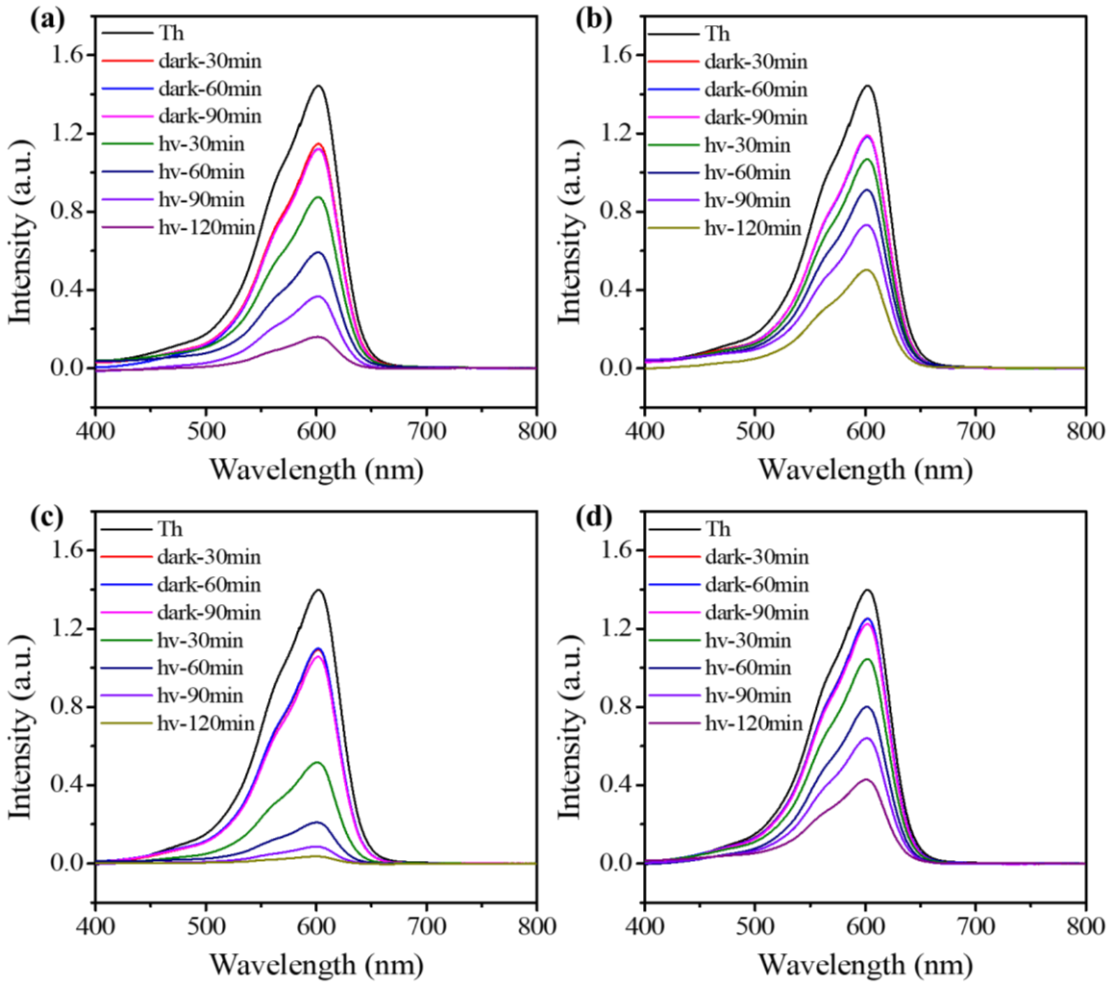

Fig. S26 UV-Vis spectra recorded for **Th** degradation experiments catalyzed by **P-CON** (a), **P-COF** (b), **T-CON** (c), and **T-COF** (d).

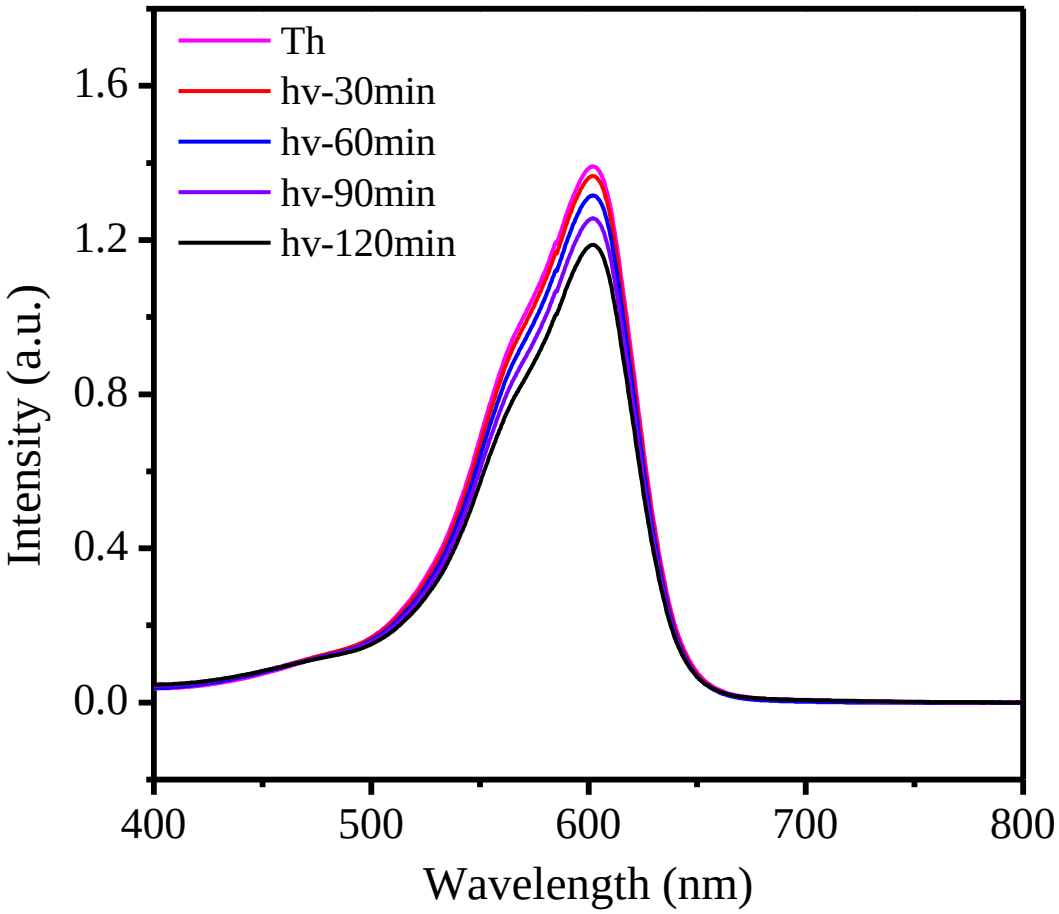

Fig. S27 UV-Vis spectra of a **Th** aqueous solution under visible light irradiation for different time.

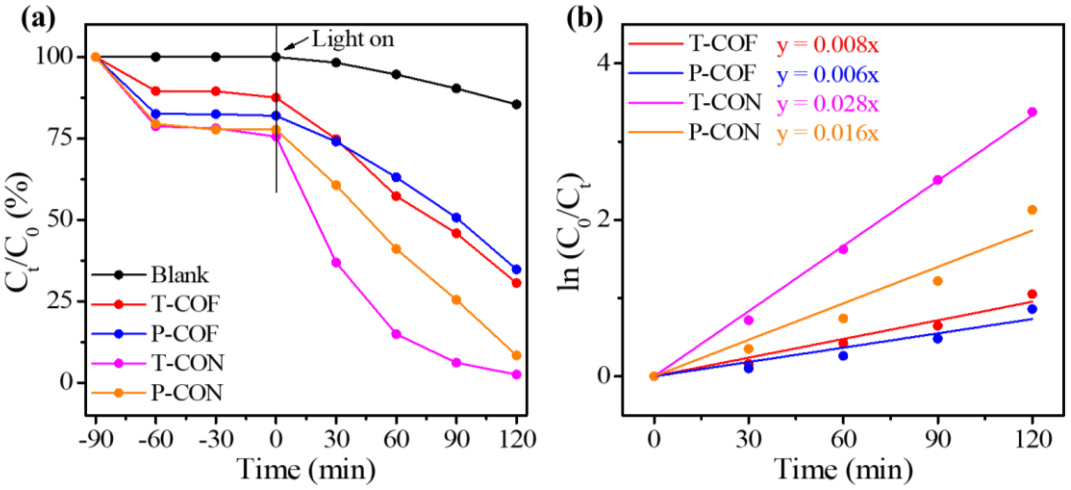

Fig. S28 Photocatalytic degradation performance of the COFs and CONs for **Th** degradation under visible light irradiation for different time (a), and pseudo-first-order kinetic curves of the photocatalytic degradation experiments (b).

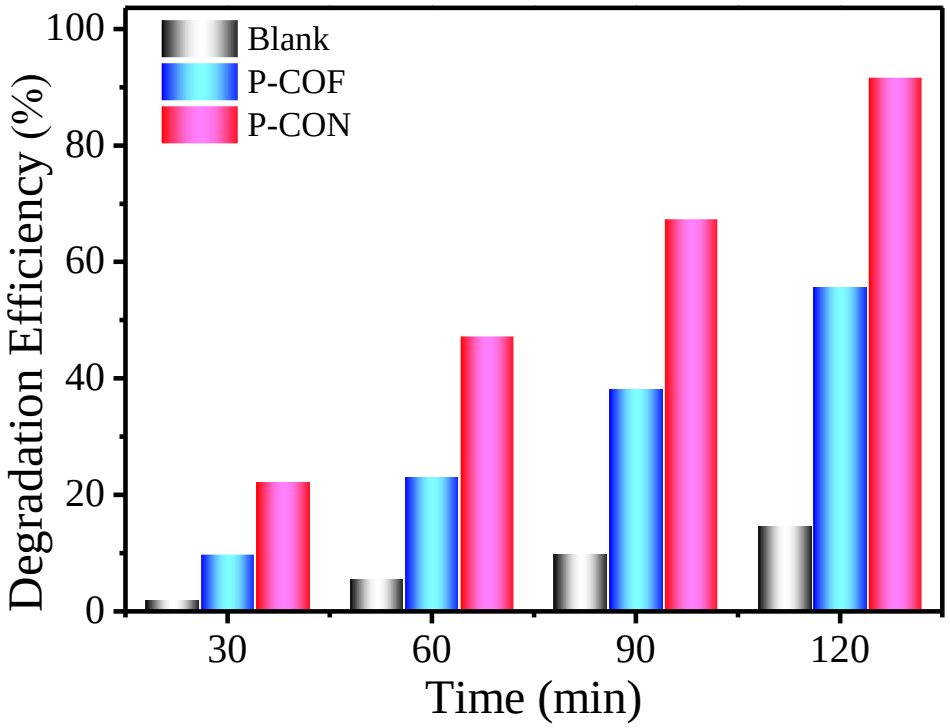

Fig. S29 Comparison of photocatalytic efficiency of **blank**, **P-COF** and **P-CON** for **Th** degradation during different time.

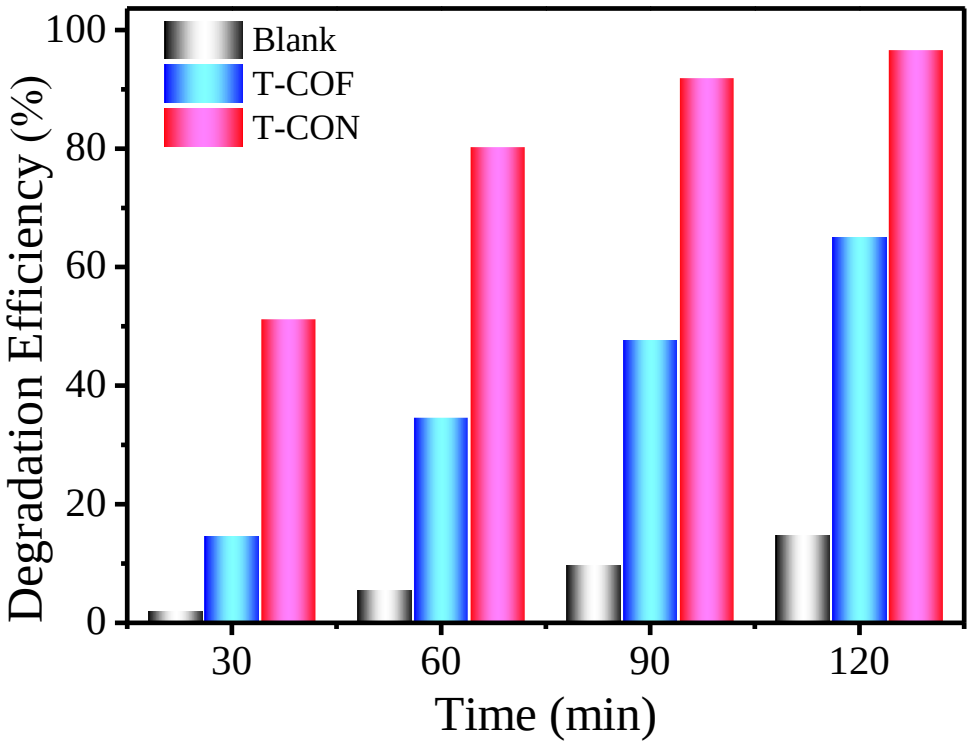

Fig. S30 Comparison of photocatalytic efficiency of **blank**, **T-COF** and **T-CON** for **Th** degradation during different time.

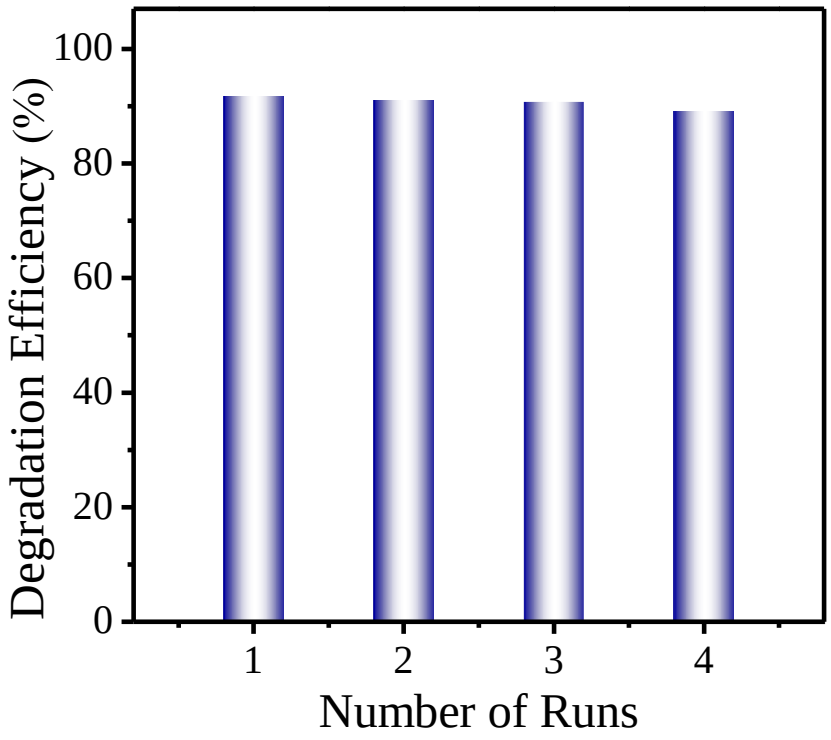

Fig. S31 Cyclic efficiency of **P-CON** for **Th** degradation.

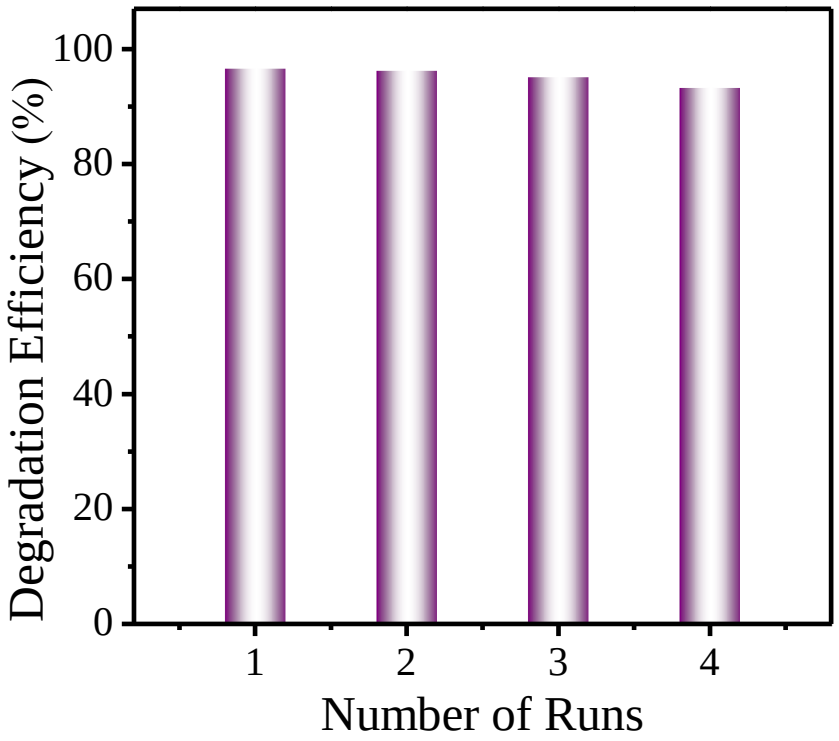

Fig. S32 Cyclic efficiency of **T-CON** for **Th** degradation.

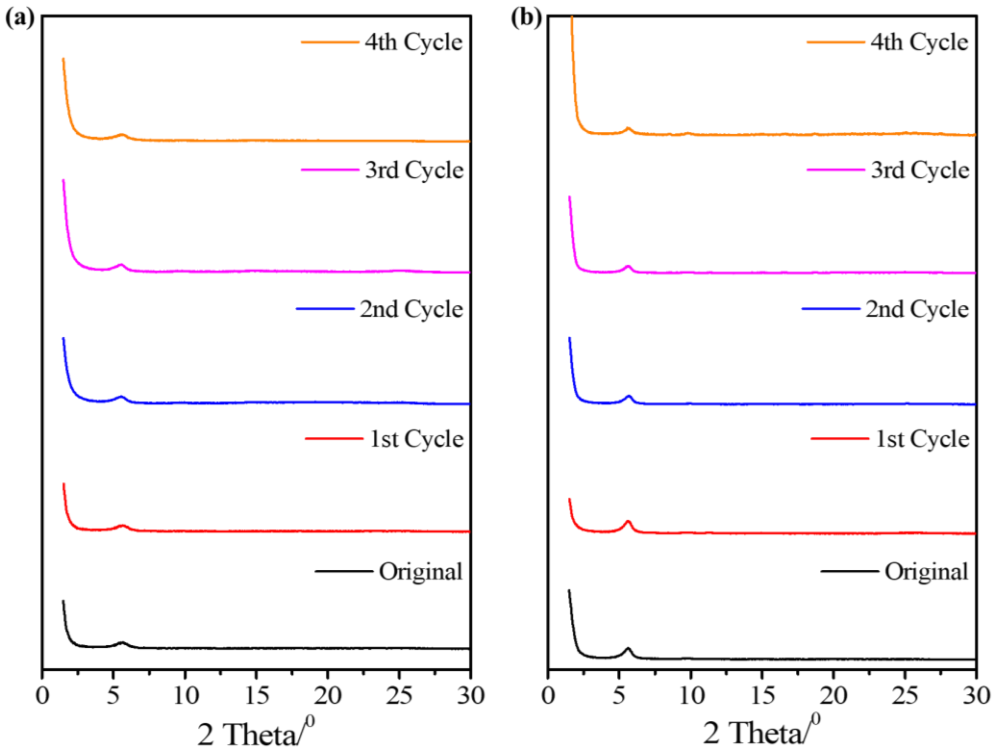

Fig. S33 PXRD patterns of **P-CON** (a) and **T-CON** (b) used for **Th** degradation after each cycle.

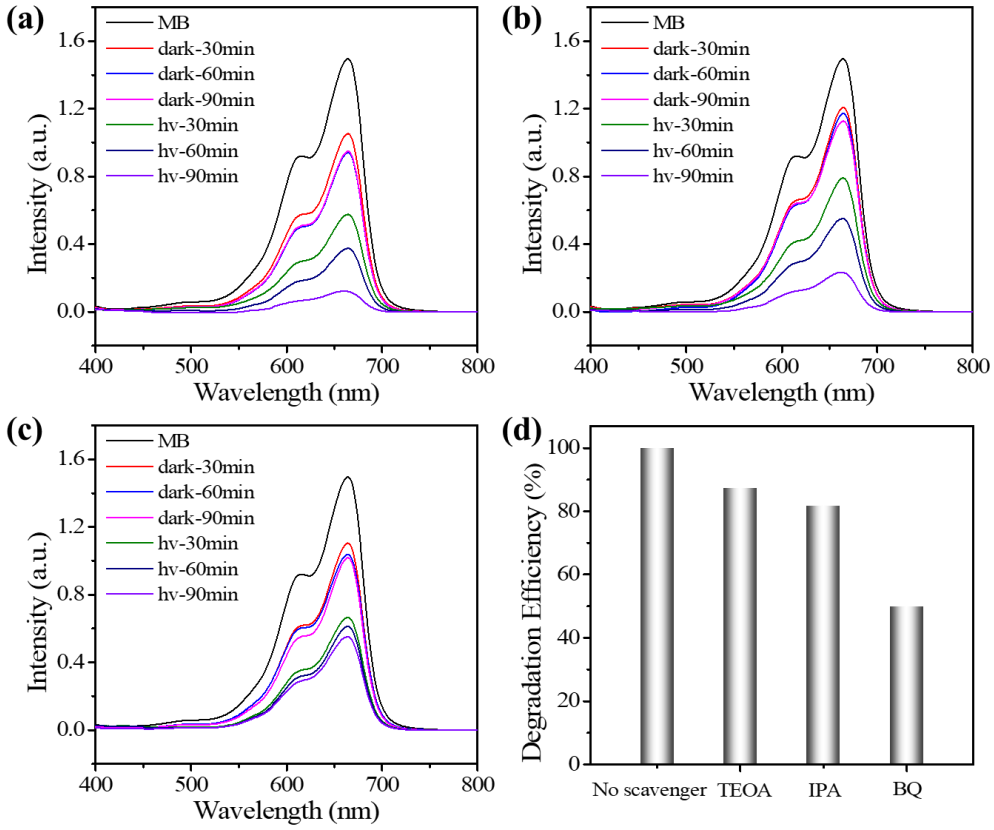

Fig. 34 UV-vis spectra recorded for MB degradation experiments catalyzed by T-CON in the presence of different kinds of scavengers: (a) **TEOA**; (b) **IPA**; (c) **BQ**. (d) Effect of different scavengers, **TEOA**, **IPA** and **BQ** on the photocatalytic degradation of **MB** by **T-CON** under visible light irradiation for 90 min.

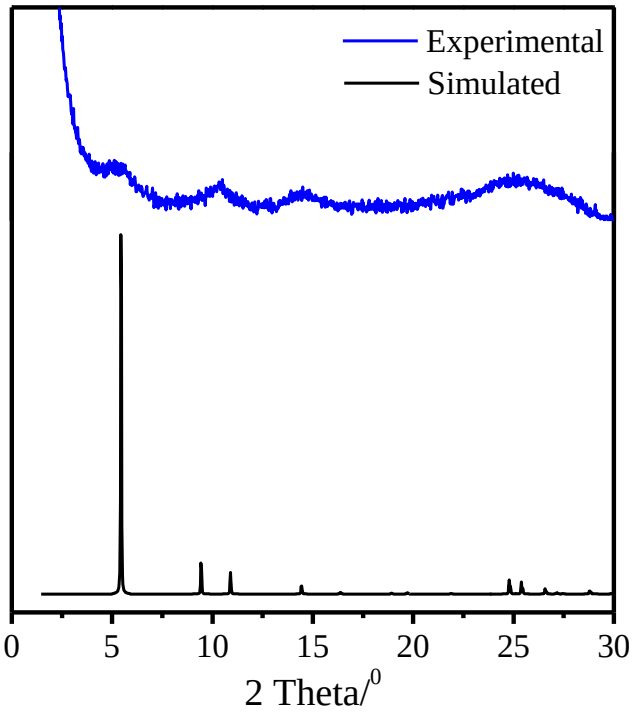

Fig. S35 Comparison between the experimental PXRD pattern of **Tp-P-CON** (blue) and the simulated PXRD pattern of its corresponding COF with eclipsed stacking (black).

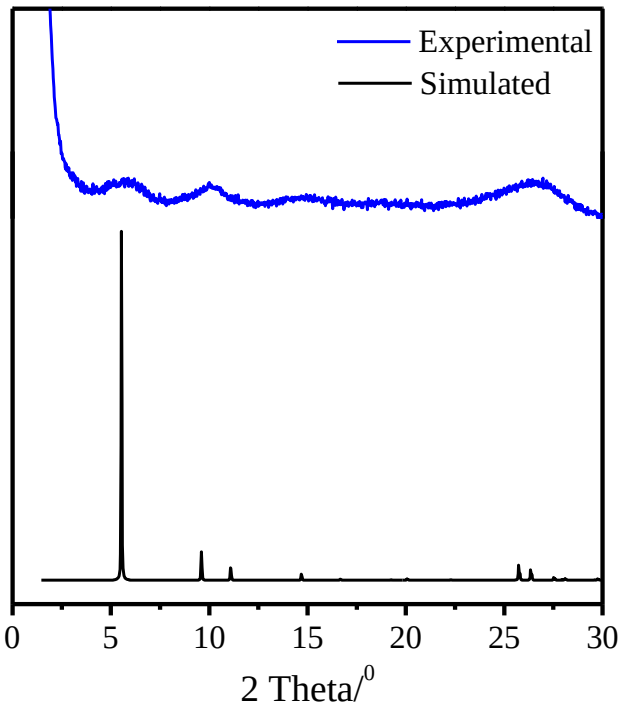

Fig. S36 Comparison between the experimental PXRD pattern of **Tp-T-CON** (blue) and the simulated PXRD pattern of its corresponding COF with eclipsed stacking (black).

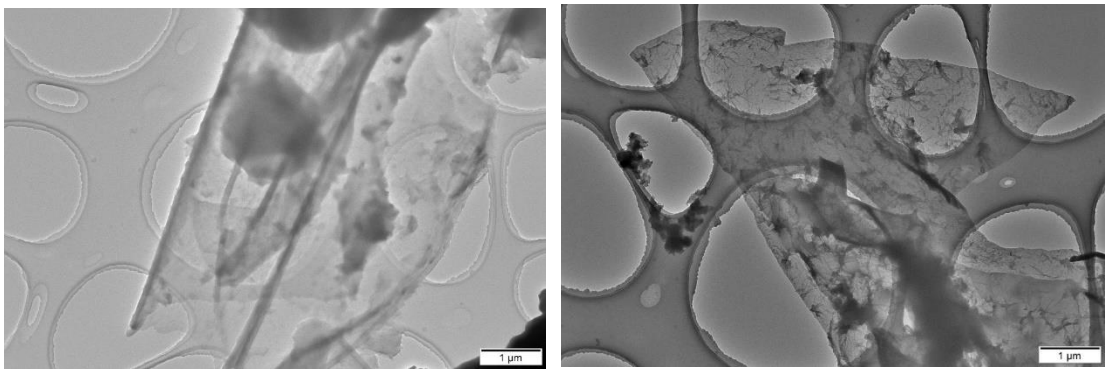

Fig. S37 TEM images of **Tp-P-CON and Tp-T-CON**.

Table S1 Fractional atomic coordinates for the unit cell of **P-COF** with AA stacking.

P3				
a = b = 18.55 Å, c = 3.60 Å, α = β = 90.00° and γ = 120°				
1	C1	0.75269	-0.6293	0.59458
2	C2	0.71674	-0.57822	0.58831
3	C3	0.76702	-0.48913	0.55531
4	C4	0.84891	-0.45019	0.39985
5	C5	0.89497	-0.36534	0.3587
6	C6	0.86351	-0.31361	0.46484
7	C7	0.78343	-0.35081	0.62157
8	C8	0.73652	-0.43543	0.66786
9	N9	0.91263	-0.22735	0.41618
10	C10	0.88541	-0.17537	0.39728
11	C11	0.94454	-0.08699	0.38955
12	C12	1.03077	-0.05393	0.38817
13	H13	0.8207	-0.59971	0.58483
14	H14	0.87536	-0.48792	0.29873
15	H15	0.95728	-0.33776	0.23415
16	H16	0.75747	-0.3122	0.71656
17	H17	0.67507	-0.46113	0.79924
18	H18	0.81887	-0.19453	0.39868
19	H19	1.05546	-0.09673	0.3906

Table S2 Fractional atomic coordinates for the unit cell of **T-COF** with AA stacking.

P3				
a = b = 18.32 Å, c = 3.61 Å, α = β = 90.00° and γ = 120°				
1	C1	0.75363	-0.63004	0.40073
2	C2	0.71848	-0.57725	0.40964
3	C3	0.77034	-0.48742	0.45592
4	C4	0.85267	-0.4502	0.61591
5	C5	0.89984	-0.3648	0.67246
6	C6	0.86907	-0.31087	0.57843
7	C7	0.78856	-0.34632	0.41763
8	C8	0.74065	-0.4314	0.35552
9	N9	0.91922	-0.22411	0.6423
10	C10	0.89187	-0.17137	0.67188
11	C11	0.95172	-0.0822	0.68493
12	N12	1.0348	-0.04928	0.68398
13	H13	0.82237	-0.601	0.4142
14	H14	0.87857	-0.48975	0.70858
15	H15	0.96251	-0.33859	0.79955
16	H16	0.76299	-0.30601	0.33207
17	H17	0.67892	-0.45559	0.22196
18	H18	0.82472	-0.19004	0.67235